Comprehensive study of the three- and four-neutron systems at low energies

Michael D. Higgins [*]
Department of Physics and Astronomy, Purdue University, West Lafayette, Indiana 47907, USA

Chris H. Greene [†]
Department of Physics and Astronomy, Purdue University, West Lafayette, Indiana 47907, USA
and Purdue Quantum Science and Engineering Institute, Purdue University, West Lafayette, Indiana 47907, USA

A. Kievsky [‡] and M. Viviani [§]
Instituto Nazionale di Fisica Nucleare, Largo Pontecorvo 3, 56127 Pisa, Italy

(Received 23 November 2020; accepted 12 February 2021; published 25 February 2021)

This work presents further analysis of the three- and four-neutron systems in the low energy regime using adiabatic hyperspherical methods. In our previous article [M. D. Higgins *et al.*, Phys. Rev. Lett. **125**, 052501 (2020)], the low-energy behavior of these neutron systems was treated in the adiabatic approximation, neglecting the off-diagonal nonadiabatic couplings. A thorough analysis of the density of states through a multichannel treatment of the three-and four-neutron scattering near the scattering continuum threshold is performed, showing no evidence of a $4n$ resonance at low energy. A detailed analysis of the long-range behavior of the lowest few adiabatic hyperspherical potentials shows there is an attractive ρ^{-3} universal behavior which dominates in the low-energy regime of the multichannel scattering. This long-range behavior leads to a divergent behavior of the density of state for $E \to 0$ that could account for the low-energy signal observed in the 2016 experiment by Kisamori *et al.* [Phys. Rev. Lett. **116**, 052501 (2016)].

DOI: 10.1103/PhysRevC.103.024004

I. INTRODUCTION

Few-neutron systems have been the subject of interest over the past couple of decades due to the possibility of forming low-energy bound states or temporary bound states through a long-lived resonance in the scattering continuum. The interest in these systems arose from experimental evidence of a possible low-energy tetraneutron ($4n$) state, most notably from experiments performed by Marqus *et al.* in 2002 [1] in the reaction ${}^{14}_{4}\mathrm{Be} \to {}^{10}_{4}\mathrm{Be} + 4n$ and in a more recent experiment by Kisamori *et al.* in 2016 [2] in the nuclear reaction ${}^{4}_{2}\mathrm{He} + {}^{8}_{2}\mathrm{He} \to {}^{8}_{4}\mathrm{Be} + 4n$. The interpretation of the results in these experiments sparked numerous theoretical studies into whether four interacting neutrons can bind or produce a resonance with current nuclear models [3–17].

The experiment by Marqus *et al.* in 2002 lead to a number of theoretical investigations into whether a $4n$ state could exist [3–7]. These theoretical studies have shown that, with current nuclear models, a $4n$ bound state could not exist. Only with a modification to the nuclear Hamiltonian, either via an additional four-body interaction [3] or other unrealistic enhancement of the nucleon-nucleon (NN) two-body interactions could a $4n$ bound state exist. Changes made to the well established nuclear Hamiltonians, such as the AV18/IL2 model in [4], results in overbinding in many light nuclei and even leads to a dineutron bound state.

Most theoretical studies that came out as a result of this 2002 experiment concluded that a $4n$ bound state or resonance could not exist with current nuclear theory. However, a more recent experiment by Kisamori *et al.* in 2016 shows evidence of a possible $4n$ resonance measured at an energy of $0.83 \pm 0.65(\mathrm{stat.}) \pm 1.25(\mathrm{sys.})$ MeV [2] above the four-body continuum. This most recent experiment sparked a renewed theoretical interest in this question [8–17]. Some of these more recent theoretical studies agree with the earlier studies that a $4n$ bound or resonant state is unsupported by current theoretical models [11–17], while other studies confirm the possible existence of a $4n$ state as depicted in the 2016 experiment [8–10]. This disagreement over whether a $4n$ state exists warrants further study of the low-energy scattering of few neutrons in the continuum, thus providing motivation for our most recent work published in *Physical Review Letters* [18].

In that work, we solve the trineutron ($3n$) and tetraneutron ($4n$) systems using the adiabatic hyperspherical framework, which has been successful at predicting resonances in few-body atomic systems in both a qualitative manner through the structure of the adiabatic potentials and quantitatively through an analysis of the phase shift [19,20]. These few-neutron systems were studied primarily in the adiabatic approximation, neglecting nonadiabatic couplings to the excited states. The lowest adiabatic potentials in both $3n$ and $4n$ systems are purely repulsive and qualitatively show no features to support a bound or resonant state above the scattering continuum.

[*] higgin45@purdue.edu
[†] chgreene@purdue.edu
[‡] alejandro.kievsky@pi.infn.it
[§] michele.viviani@pi.infn.it

In addition, an elastic phase shift analysis was performed for the lowest adiabatic potential with the second-derivative diagonal nonadiabatic correction that showed no features of a resonance at low energy, only an enhancement of the density of states caused largely by an attractive ρ^{-3} long-range feature in the potential as it approaches the noninteracting limit. We attribute the low-energy signal seen in the Kisamori *et al.* experiment to this enhancement, and not to a resonant $4n$ state [18]. The purpose of this article is to expand on this previous work to investigate the effects of nonadiabatic couplings to the excited states on this low-energy behavior in a more comprehensive multichannel scattering treatment of these systems.

The rest of this article is organized in the following way. Section II provides details on the adiabatic hyperspherical approach, including the numerical techniques used to compute the nonadiabatic couplings. The lowest few adiabatic hyperspherical potential curves for both $3n$ and $4n$ systems are reported in Sec. III, showing the repulsive nature of few interacting neutrons, with an emphasis on the lowest potential in both systems. In Sec. IV, the nonadiabatic couplings are shown for the lowest few channels to provide qualitative and some quantitative features of the long-range behavior. Section V gives a detailed analysis of the long-range behavior of the lowest few adiabatic potentials, specifically providing the scattering length dependence of the ρ^{-3} coefficient in these potentials at long range. With knowledge of the long-range behavior of the adiabatic potentials and nonadiabatic couplings, a multichannel treatment of the scattering of few-neutron systems above the continuum is performed in Sec. VI and compared with the adiabatic treatment. Last, Sec. VII presents our conclusions.

II. ADIABATIC HYPERSPHERICAL APPROACH

The $3n$ and $4n$ nuclear systems are explored in the framework of the hyperspherical representation. The main advantage of using this representation to study these few-body systems is that all of the dynamical features of the interparticle interactions and reaction pathways at different length scales can be described both qualitatively and quantitatively on an equal footing through an adiabatic parameter denoted the hyperradius. Another key advantage of using the hyperspherical representation comes from its success in predicting resonances in few-body atomic systems. For example, photodetachment resonance in the positronium negative ion above the $n = 2$ threshold was predicted by Botero and Greene in 1986 [19] and confirmed by experiment in 2016 [21], and shape resonances in the e-H system were predicted by Lin in 1975 [20] and confirmed by experiment in 1977 [22]. In both of these theoretical studies, the resonance features were observed both qualitatively in the structure of the adiabatic potential curves as well as quantitatively through an analysis of the elastic phase shifts.

A. Theoretical formulation

Within the adiabatic hyperspherical approach the $3n$ and $4n$ systems are solved using both an explicitly correlated Gaussian [23–26] (CGHS) basis and the hyperspherical harmonic (HH) basis ([24] and references therein). The Hamiltonian for most systems can separate the center-of-mass coordinates from the relative coordinates, $\hat{H} = \hat{H}_{\rm CM} + \hat{H}_{\rm rel.}$. The center-of-mass Hamiltonian contains the kinetic energy operator of the center of mass. The Hamiltonian of the relative motion contains the relative hyperradial and hyperangular kinetic energy operators, as well as the potential energy.

The hyperangular kinetic energy and potential energy operators make up the adiabatic Hamiltonian, with the hyperradius treated initially as an adiabatic parameter. The generalized N-body adiabatic eigenvalue equation in hyperspherical coordinates to be solved is

$$H_{ad}(\rho, \Omega)\Phi_\nu(\rho, \Omega) = U_\nu(\rho)\Phi_\nu(\rho, \Omega), \tag{1}$$

where ρ is the hyperradius, Ω is a set of hyperangles, ν is an index that labels the eigenstates of $H_{ad}(\rho, \Omega)$, and

$$H_{ad}(\rho, \Omega) = \frac{\hbar^2}{2\mu\rho^2}\left[\Lambda^2 + \frac{(3N-4)(3N-6)}{4}\right] + V_{\rm int.}(\rho, \Omega), \tag{2}$$

where μ is the hyperradial reduced mass, which can be arbitrarily defined with an appropriate rescaling of the hyperradius and taken here to be $m/2$, where m is the neutron mass. The operator Λ represents the hyperangular grand-angular momentum of the system and $V_{\rm int.}(\rho, \Omega)$ is the potential operator between the nucleons, containing two-body and three-body interaction terms.

The CGHS basis is used to diagonalize the adiabatic Hamiltonian given by Eq. (2), which includes all particle interactions. The HH basis forms a complete basis that consists of eigenfunctions of the hyperangular grand-angular momentum squared operator Λ^2 labeled by an angular-momentum quantum number (see Appendix B of [24] and references therein), denoted here as K. The state label ν in Eq. (1) corresponds to an eigenstate of the adiabatic Hamiltonian, as stated above. In the noninteracting limit, this label ν is equivalent to K for the HH basis, with $\nu = 1$ corresponding to the lowest HH compatible with symmetry, spin, and angular momentum having $K = 1$ in the $3n$ case (for $J^\pi = \frac{3}{2}^-$) and $K = 2$ for the $4n$ (for $J^\pi = 0^+$). In addition, it should be noted that the noninteracting eigenstates of $H_{ad}(\rho, \Omega)$ are in one-to-one correspondence with the states of a d-dimensional isotropic harmonic oscillator, which are known to have a very high degeneracy that increases rapidly with dimensionality (for an example in the case of noninteracting fermions, see [27]).

The full N-body wave function in the relative coordinates is expanded in the eigenstates of Eq. (1), giving the ansatz

$$\Psi_E(\rho, \Omega) = \rho^{-\frac{3N-4}{2}} \sum_\nu F_{E,\nu}(\rho)\Phi_\nu(\rho, \Omega). \tag{3}$$

The factor $(3N-4)(3N-6)/4$ in Eq. (2) comes from the multiplying factor of ρ in Eq. (3), which eliminates the first derivative in the hyperradial kinetic energy. Applying $\hat{H}_{\rm rel.}$ to Eq. (3), projecting from the left with $\Phi_{\nu'}(\rho, \Omega)$, and integrating over the hyperanglular coordinates and tracing over spin degrees of freedom leads to the following coupled hyperradial

Schrödinger equations:

$$\left(-\frac{\hbar^2}{2\mu}\frac{\partial^2}{\partial\rho^2}+W_\nu(\rho)-E\right)F_{\mathrm{E},\nu}(\rho) - \frac{\hbar^2}{2\mu}\sum_{\nu'\neq\nu}\left(2P_{\nu\nu'}(\rho)\frac{\partial}{\partial\rho}+Q_{\nu\nu'}(\rho)\right)F_{E,\nu'}(\rho)=0, \quad (4)$$

where $P_{\nu\nu'}(\rho)$ and $Q_{\nu\nu'}(\rho)$ are first and second derivative nonadiabatic coupling matrix elements and $W_\nu(\rho)=U_\nu(\rho)-\frac{\hbar^2}{2\mu}Q_{\nu\nu}(\rho)$ is the νth effective adiabatic potential [28–30].

Once Eq. (1) is solved for $U_\nu(\rho)$ and normalized fixed-ρ eigenfunction $\Phi_\nu(\rho,\Omega)$, the next step is to calculate the first- and second-derivative nonadiabatic coupling matrix elements defined as [28]

$$P_{\mu\nu}(\rho)=\left\langle\Phi_\mu\left|\frac{\partial\Phi_\nu}{\partial\rho}\right.\right\rangle, \quad (5)$$

$$Q_{\mu\nu}(\rho)=\left\langle\Phi_\mu\left|\frac{\partial^2\Phi_\nu}{\partial\rho^2}\right.\right\rangle, \quad (6)$$

where the integrals are over the hyperangles. Symmetry properties of the P matrix elements can be derived from manipulating Eq. (5). By differentiating the overlap $\langle\Phi_\mu|\Phi_\nu\rangle$ with respect to ρ, it can be shown through Eq. (5) that $P_{\mu\nu}(\rho)=-P_{\nu\mu}(\rho)$ and $P_{\nu\nu}(\rho)=0$. The diagonal second derivative coupling term added to the lowest adiabatic potential, $W_1(\rho)$, provides an upper bound to the ground state, thus is important to include.

B. Nondiabatic coupling: Numerical approach

The diagonal second-derivative couplings can be re-written as $Q_{\nu\nu}(\rho)=-\langle\frac{\partial\Phi_\nu}{\partial\rho}|\frac{\partial\Phi_\nu}{\partial\rho}\rangle$, thus one needs to only compute $\frac{\partial\Phi_\nu}{\partial\rho}$. One standard way to compute this derivative is to use finite-difference methods, however, we use a different approach that involves solving a matrix equation. The idea is to multiply Eq. (1) by ρ^2 then differentiate with respect to ρ. This leads to the following matrix equation [28,31]:

$$\rho^2[U_\nu(\rho)-H_{ad}(\rho,\Omega)]\chi_\nu(\rho,\Omega) = \left[\frac{\partial}{\partial\rho}[\rho^2H_{ad}(\rho,\Omega)]-\frac{\partial}{\partial\rho}[\rho^2U_\nu(\rho)]\right]\Phi_\nu(\rho,\Omega), \quad (7)$$

where

$$\chi_\nu(\rho,\Omega)=\frac{\partial}{\partial\rho}\Phi_\nu(\rho,\Omega)+c\Phi_\nu(\rho,\Omega) \quad (8)$$

and c is solved for in an iterative process until the derivative only changes by a small amount, using the fact that $P_{\nu\nu}(\rho)=0$.

Once the derivative of the channel functions are determined, the first-derivative coupling elements can be computed easily from Eq. (5). In general, the second derivatives of the channel functions are required to compute the second-derivative matrix elements, as indicated by Eq. (6). To avoid computing the second derivative of the channel functions, the second-derivative couplings can be expressed in terms of the derivatives of the first-derivative matrix elements and channel functions through the relation [28]

$$Q_{\mu\nu}(\rho)=\frac{\partial}{\partial\rho}P_{\mu\nu}(\rho)-\left\langle\frac{\partial\Phi_\mu}{\partial\rho}\middle|\frac{\partial\Phi_\nu}{\partial\rho}\right\rangle. \quad (9)$$

However, it has been shown that, when solving the coupled hyperradial equations in Eq. (4) by R-matrix propagation with the slow-variable discretization (SVD) method, only the component $-\langle\frac{\partial\Phi_\mu}{\partial\rho}|\frac{\partial\Phi_\nu}{\partial\rho}\rangle$ of $Q_{\mu\nu}(\rho)$ is needed (see Appendix B of [28]). Therefore, throughout the rest of this article, any further mention of second-derivative couplings refer to this component.

III. ADIABATIC POTENTIALS

The adiabatic hyperspherical potentials were obtained using two different basis expansions, the HH basis and the CGHS basis, along with different nuclear models for the two-body interactions. The primary calculations were performed using the AV18 and AV8′ [23,32] two-body nuclear potentials. Other nuclear interaction models are used with the HH basis to show a comparison of the adiabatic potentials among the various theories. The other NN interactions include the local NN potential model NVIa for the $3n$ system and models NVIa and NVIb for the $4n$ system, derived within the chiral effective field theory approach [33,34]. The potentials were obtained for symmetries $J^\pi=0^+$ and $\frac{3}{2}^-$ for the $4n$ and $3n$ systems, respectively, providing the most attraction between the neutrons. The lowest few potentials, including the second-derivative nonadiabatic coupling term, for both $3n$ and $4n$ systems are shown in Fig. 1 using the AV8′ interaction.

The lowest potentials in both systems exhibit important features that aid in our understanding of the interaction between multiple neutrons. It is most evident from the potentials shown in Fig. 1 that no bound or resonant states are supported for either the $3n$ or $4n$ system. There is no potential minimum or potential barrier that can support a bound or even temporarily bound resonant state that would indicate the existence of a trineutron or tetraneutron state. In fact, over the entire range of hyperradii, the potentials are purely repulsive due in part to the large Pauli repulsion in these fermionic systems. However, there is still significant attraction in these systems, which can be seen from a comparison with the noninteracting potential (dashed curves) in Fig. 1. The lowest few adiabatic potentials lie well below the noninteracting potentials over a large range in the hyperradius, with the greatest attraction evident in the lowest potentials for both systems.

The long-range behavior of the adiabatic potentials plays an important role in determining the low-energy behavior of the scattering phase shift. From Fig. 1, the lowest few adiabatic potentials in both neutron systems approach the noninteracting potentials as ρ^{-3}. It is found that the asymptotic form of the lowest few potentials take the form

$$W_\nu(\rho)\to\frac{\hbar^2}{2\mu}\left(\frac{l_{\mathrm{eff}}(l_{\mathrm{eff}}+1)}{\rho^2}+\frac{C_{3,\nu}}{\rho^3}\right), \quad (10)$$

where l_{eff} is the effective angular momentum quantum number, and where $C_{3,\nu}=C_\nu a$, with a being the s-wave scattering length, and C_ν is a dimensionless constant that depends on

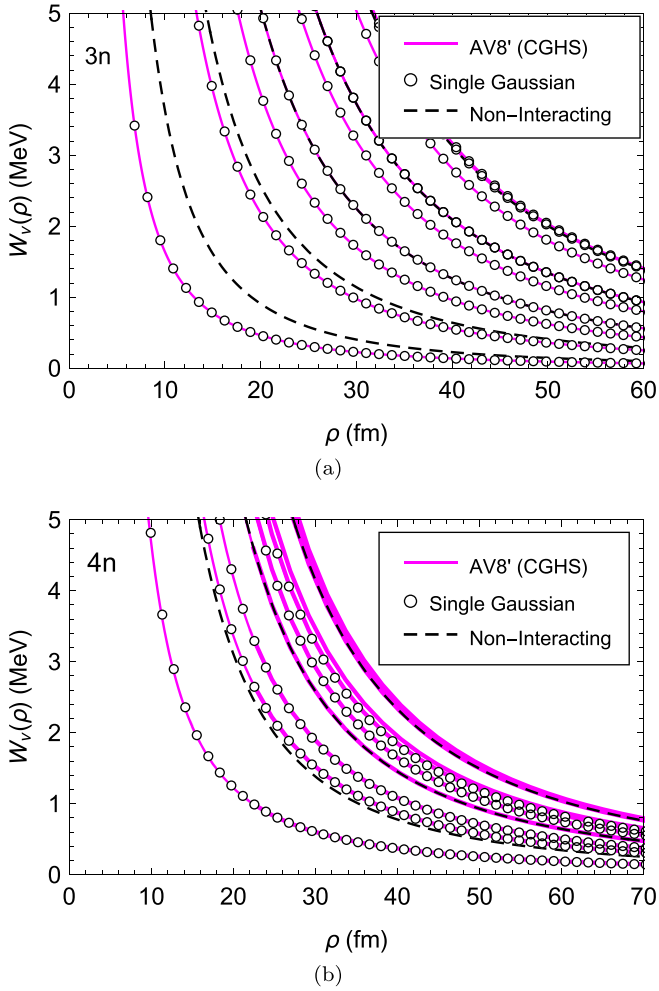

FIG. 1. The lowest few adiabatic potentials for the $3n$ (a) and $4n$ (b) systems using the AV8′ two-body interaction are presented with the ordering of states from bottom to top, with the lowest curve representing $\nu = 1$. The diagonal second-derivative nonadiabatic couplings are included. The noninteracting potentials (dashed lines) are shown to provide a qualitative picture of the amount of attraction in these systems. Also, the adiabatic potentials are compared to a single-Gaussian model (open circles) with $L = 0$ and $L = 1$ natural parity states for the $4n$ and $3n$ systems, respectively.

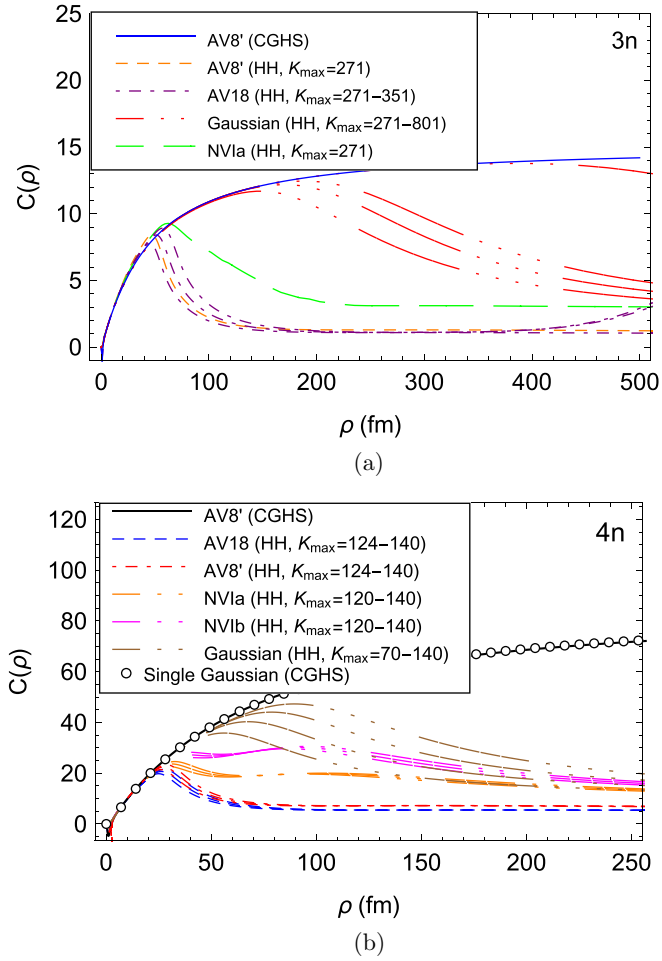

FIG. 2. Plots of the dimensionless function $C_\nu(\rho) \equiv (\rho/a)[\rho^2 W_\nu(\rho) 2\mu/\hbar^2 - l_{\rm eff}(l_{\rm eff}+1)]$ for the $3n$ (a) and $4n$ (b) systems with $\nu = 1$. According to Eq. (10), we should obtain $C_\nu(\rho \to \infty) = C_\nu$, where C_ν is the coefficient listed in Table II. We observe the slow convergence for large ρ of the adiabatic potentials calculated using the HH basis, with increasing values of $K_{\rm max}$ indicated as higher curves for each nuclear model that tends towards the most converged CGHS calculation. However, it has to be noted that where the convergence is achieved, the functions $C_\nu(\rho)$ obtained for the different interactions used in this work almost collapse onto a single curve. Noticeably, this happens already for fairly small values of rho, showing that the adiabatic potentials are already universal at moderate values of the hyperradius. In fact, the limit $C_\nu(\rho) = C_\nu$ is reached only for $\rho > 500$ fm.

system size, symmetry, and eigenstate. For the lowest adiabatic potential, the ρ^{-3} behavior is emphasised through a plot, shown in Fig. 2, of $C(\rho) = (\rho/a)[(2\mu/\hbar^2)W_1(\rho) - l_{\rm eff.}(l_{\rm eff.}+1)]$ with $l_{\rm eff.} = 5$ for the lowest potential of the $4n$ system and $l_{\rm eff.} = 5/2$ for the lowest $3n$ potential. These have been rescaled by the spin-singlet s-wave scattering length. Figure 2 shows a comparison of $C(\rho)$ for both neutron systems obtained for different nuclear interaction models and basis sets. In particular, these figures show the slow convergence of the HH basis at large values of the hyperradius compared to calculations performed using the CGHS basis, which provides the best converged results beyond 30–50 fm. At small hyperradii, both basis sets are well converged and the potential curves computed with different nuclear interaction models are nearly indistinguishable. Only at large hyperradii is there a clear difference in the lowest potential, which is largely due to the slow convergence of the HH basis.

Universal behavior is observed in these few-neutron systems, as shown by the remarkable agreement between the adiabatic potentials in Fig. 1 using both the accurate and well established AV8′ nuclear interaction and a single Gaussian potential, whose parameters are given in Table I. This agreement resulting from two qualitatively different interactions demonstrates that interacting neutrons exhibit long-range universal physics, further supported by similarities in the elastic phase shifts [18]. This can be understood due to the large ratio of the singlet s-wave scattering length to the range of the nuclear

TABLE I. Single-Gaussian parameters used for singlet and triplet two-body interactions. The parameters were extracted from fits to the central component of the AV8′ potential. The parameter V_u is the strength at unitarity.

State	V_0(MeV)	V_u(MeV)	r_0(fm)
^1S	−31.7674	−35.1265	1.7801
^3P	95.7280	−646.625	0.8809

interaction, which is approximately $|a_s/r_0| \approx 10$. The connection between short-range interactions with large scattering lengths to universal physics has been extensively studied in various contexts relating to not only the Efimov effect in atomic and nuclear three-body systems [24,35–44], but also in connection to BCS-BEC crossover in few-fermion atomic systems [24,45,46]. Furthermore, the $3n$ and $4n$ adiabatic potentials using different and well established nucleon-nucleon interactions are universal at moderately small hyperradii (from 5–30 fm), with qualitative differences in the range $0 < \rho < 5$ fm, as seen in Fig. 2. This universal behavior in these neutron few-body systems is explored further in Sec. V, analyzing the long-range behavior of these adiabatic potentials at different scattering lengths up to unitarity.

One key interest concerning the neutron-neutron interaction is the role of tensor and spin-orbit interactions for systems of few neutrons. In nucleon-nucleon interactions, the tensor and spin-orbit interactions are important for binding the neutron and proton in the spin-triplet and isospin-singlet state [32]. For neutron systems, on the other hand, the tensor and spin-orbit interactions do not lead to binding of two neutrons. However, these interactions do provide extra attraction at short-range ($0 < \rho < 4$ fm). This is best illustrated in Fig. 3 for the $4n$ system, showing the difference in the lowest few adiabatic potentials for $L = 0$ states with and without the tensor and spin-orbit interactions using the AV8′ nuclear interaction model.

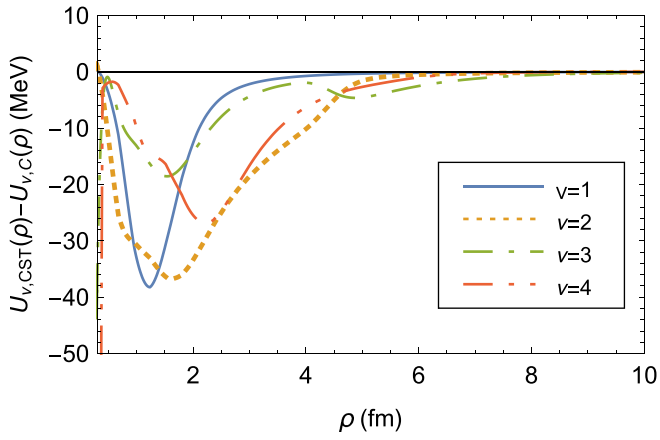

FIG. 3. Difference in the lowest few $4n$ hyperradial potentials for $L = 0$ states ($v = 1$–4) with and without the spin-orbit and tensor interactions. The differences suggest that the tensor and spin-orbit interactions provide attraction to the system at hyperradii around $0 < \rho < 5$ fm.

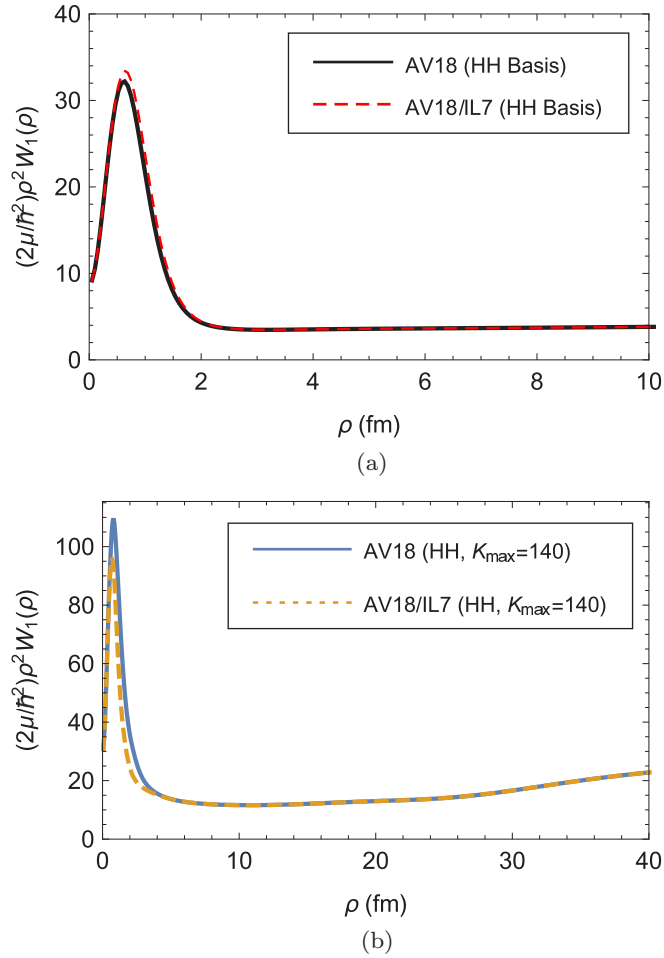

FIG. 4. A comparison of the lowest adiabatic potential using the AV18 two-body interaction with and without the IL7 3N force for the $3n$ (a) and $4n$ (b) systems. There is only a significant difference for $\rho < 5$ fm.

In many nuclear systems, the 3N force play a significant role in determining the correct binding energy of light nuclei [47–51]. Thus, a logical question would be whether or not the 3N force plays a significant role in binding of few-neutron systems. To address this question, the $3n$ and $4n$ systems were studied using the AV18 two-body potential with the Illinois 7 (IL7) model of the three-body force. A comparison between the lowest potential in both $3n$ and $4n$ systems with and without the IL7 3N term is shown in Fig. 4. As shown in Fig. 4, the lowest rescaled potentials for these systems is represented by the quantity, $(2\mu/\hbar^2)\rho^2 U(\rho)$, which approaches 30 at large ρ for the $4n$ system and 8.75 for the $3n$ system. From the comparison of this potential with and without the IL7 3N force, there is only a significant difference for $\rho < 5$ fm, with the 3N force adding slight attraction to the $4n$ system and slight repulsion in the $3n$ system. At large values of ρ, which governs the low-energy scattering of the system, the potentials are nearly identical. Thus, it is concluded the 3N force plays little role in the low-energy regime for $3n$ and $4n$ scattering with providing not enough attraction to lead to a bound or even resonant bound state.

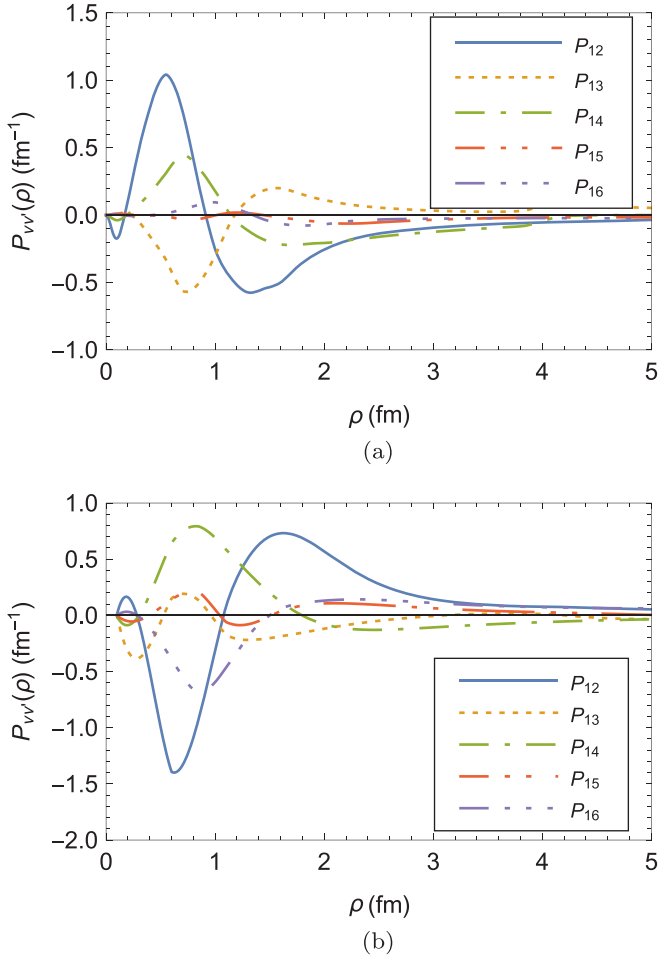

FIG. 5. The first-derivative coupling matrix elements $P_{1\nu}(\rho)$ in the lowest channel for the $3n$ (a) and $4n$ (b) systems with $\nu = 2$–6 [from Eq. (5) $P_{11}(\rho) = 0$].

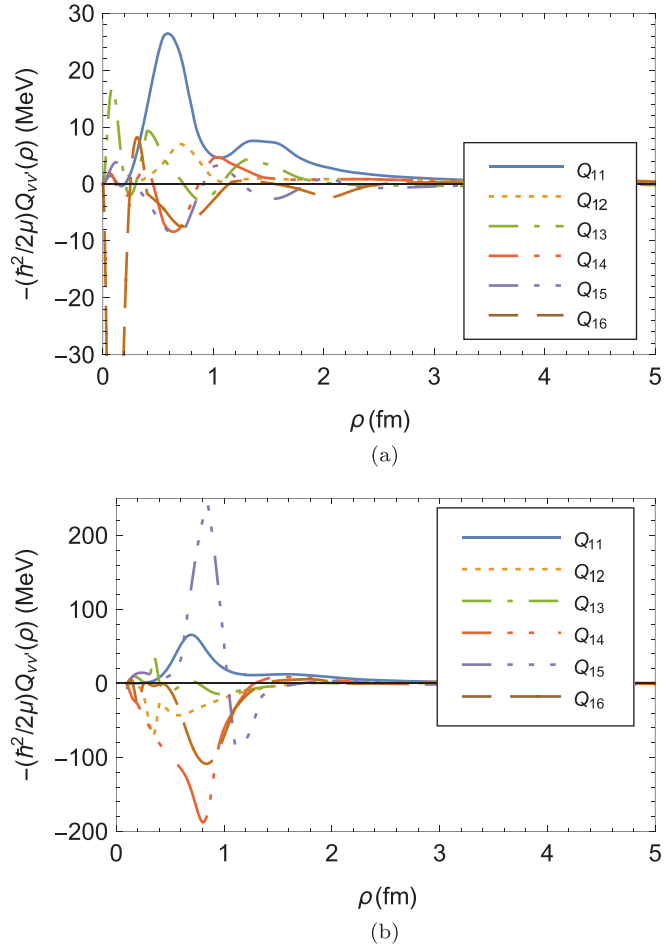

FIG. 6. The second-derivative coupling matrix elements $Q_{1\nu}$ in the lowest channel for the $3n$ (a) and $4n$ (b) systems with $\nu = 1$–6. The coupling matrix elements are scaled by $\hbar^2/2\mu$.

IV. NONADIABATIC COUPLING MATRIX ELEMENTS

Before considering the full treatment of the coupled hyperradial Schrödinger equation, the first- and second-derivative nonadiabatic coupling matrix elements need to be computed at each hyperradius. The nonadiabatic matrices, defined in Eqs. (5) and (6), are computed using the methods described in Sec. II B. The long-range behaviors of these matrix elements are analyzed with an emphasis on the nonadiabatic couplings for the $3n$ system, noting the asymptotic behavior is equivalent in the $4n$ system. Through this study, it is determined that the second-derivative coupling matrix elements fall off faster than ρ^{-3}, and do not contribute to the long-range potential given in Eq. (10). The nonadiabatic couplings between the lowest channel and lowest six channels are shown in Figs. 5 and 6 for the first- and second-derivative elements, respectively.

The first- and second-derivative couplings for the $3n$ and $4n$ systems only have a significant impact on the adiabatic potentials over a range of the hyperradius of $0 \leqslant \rho \leqslant 5$ fm, beyond which they rapidly decrease to zero. The long-range behavior of these nonadiabatic matrix elements can be seen by multiplying $P_{\mu\nu}(\rho)$ by ρ^2 and $Q_{\mu\nu}(\rho)$ by ρ^4, which is shown in Figs. 7 and 8 for the first- and second-derivative matrix elements for the $3n$ system, respectively. From these figures, it is evident the second-derivative matrix elements are

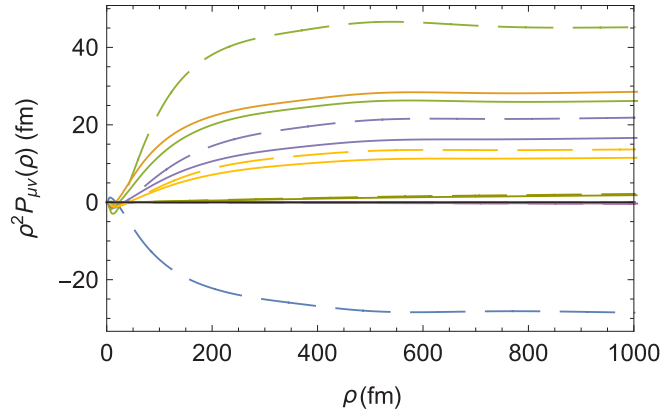

FIG. 7. The first-derivative nonadiabatic matrix elements for the lowest few $3n$ channels are shown multiplied by ρ^2 to emphasize the long-range behavior. The solid lines are the coupling matrices to the first channel and the dashed lines are coupling matrices to the second channel (i.e., $P_{1\nu}$ and $P_{2\nu}$ with $\nu = 1, \ldots, 6$).

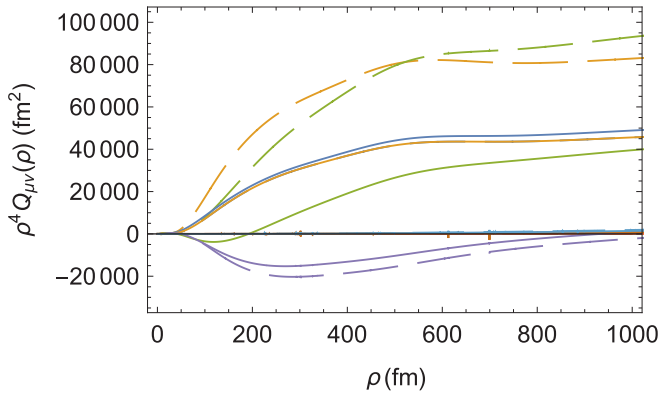

FIG. 8. The second-derivative nonadiabatic matrix elements for the lowest few $3n$ channels are shown multiplied by ρ^4 to emphasize the long-range behavior. The solid lines are the coupling matrices to the first channel and the dashed lines are coupling matrices to the second channel (i.e., $Q_{1\nu}$ and $Q_{2\nu}$ with $\nu = 1, \ldots, 6$).

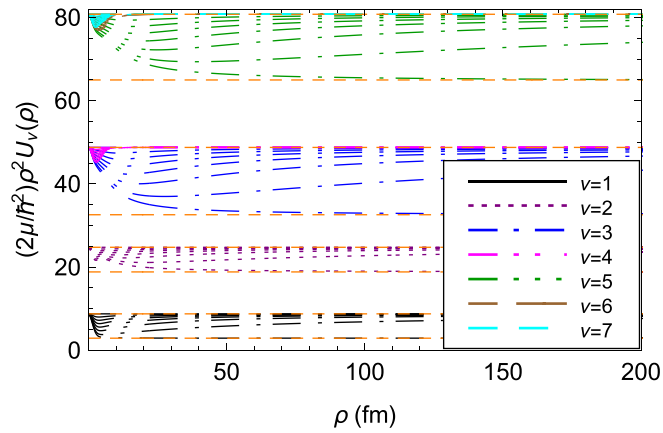

FIG. 9. The lowest 7 adiabatic potentials ($\nu = 1$–7) for the $3n$ system for the $J^\pi = \frac{3}{2}^-$ symmetry with $L = 1$ using a single-Gaussian potential with $r_0 = 1.78$ fm. The strength V_0 is tuned to give different scattering lengths from 0 to infinity with no two-body bound state. Each set of potentials represent a different s-wave scattering length in this range with limits shown by the horizontal dashed lines representing the noninteracting limit (upper dashed) and unitarity limit (lower dashed). The unitarity limits are given in Table II. The set of potentials labeled by $\nu = 1$, 2, 3, and 5 represent the potentials with the ρ^{-3} behavior as they approach the noninteracting limit and the curves labeled by $\nu = 4$, 6, and 7 represent those that fall off faster than ρ^{-3}.

short range, falling off faster than ρ^{-3}, in fact falling off as ρ^{-4}. The first-derivative matrix elements exhibit long-range behavior, falling off like ρ^{-2} at large hyperradii. Likewise, this long-range behavior in the nonadiabatic couplings is also observed in the $4n$ system.

This analysis of the long-range behavior of the nonadiabatic matrix elements indicates that the diagonal second-derivative matrix elements do not impact the long-range behavior of the adiabatic potentials, although the short-range behavior is affected. As a result, when solving the coupled hyperradial equation, the couplings only have significant influence on the collision eigenphaseshifts at high scattering energies, while the low-energy behavior is only slightly modified due to the long-range behavior of the first-derivative couplings. Section VI discusses the affect of the nonadiabatic coupling terms on the energy-dependent eigenphase shifts.

V. LONG-RANGE BEHAVIOR OF THE ADIABATIC POTENTIALS

In these few-neutron systems, it is observed that the lowest few adiabatic potentials take the form of Eq. (10), in which the potentials deviate from the noninteracting limit by a ρ^{-3} dependence that scales linearly in the two-body s-wave scattering length. This dependence of the asymptotic form on the two-body s-wave scattering length has been shown for hyperspherical potentials associated with the many particle continuum, for systems with short-range interactions having a two-body scattering length larger than the range of the interaction [52,53]. The asymptotic form is valid with and without the diagonal second derivative coupling term since the coupling terms fall off as ρ^{-4}, as was shown in Sec. IV.

To study the long-range behavior of the potentials, a single Gaussian model for the two-body interaction is used, of the form

$$V(r) = V_0 \exp\left(-\frac{r^2}{r_0^2}\right). \tag{11}$$

For a fixed range r_0, the strength V_0 is tuned to give a different s-wave scattering length, while maintaining the condition that there is no two-body bound state. The values of V_0 are chosen to give scattering lengths ranging from zero to infinity, coinciding with the noninteracting case to the unitarity regime. To represent the nn interaction, the values of V_0 and r_0 are chosen to reproduce the dominant low energy s-wave and p-wave properties produced by the spin-singlet and triplet components of the central term in the AV8′ interaction. The parameters used in the single-Gaussian calculations in Sec. III are given in Table I, along with the strength associated with the unitarity limit for the spin-singlet state denoted by V_u. To extract the expected value of $C_{3,\nu}$ for the few-neutron systems, the strength of the spin-singlet state is tuned in the range $0 < V_0 < V_u$ with r_0 fixed to the value given in the first row of Table I. The lowest few adiabatic potentials for this study are shown in Figs. 9 and 10 for the $3n$ and $4n$ systems, respectively. These figures show the lowest few potentials for 20 scattering lengths ranging from 0 to unitarity for $r_0 = 1.7801$ fm, plotted as $(2\mu/\hbar^2)\rho^2 U(\rho)$ versus ρ. Each curve approaches the value $l_{\rm eff}(l_{\rm eff}+1)$ at large ρ where, in the noninteracting limit, $l_{\rm eff} = 5/2$ for the ground state of the $3n$ $J^\pi = \frac{3}{2}^-$ system and $l_{\rm eff} = 5$ for the ground state of the $4n$ $J^\pi = 0^+$ system. The lowest of each set of curves is the unitarity potential where the strength of the interaction is tuned to give an infinite scattering length. The unitarity values for $l_{\rm eff}$ describing the long-range potential are given in Table II and labeled as $l_{\rm eff,u}$. One general and universal property of every N-particle system with finite range interactions is that the long-range hyperradial potential curves associated with the N-body continuum can often (but not necessarily always)

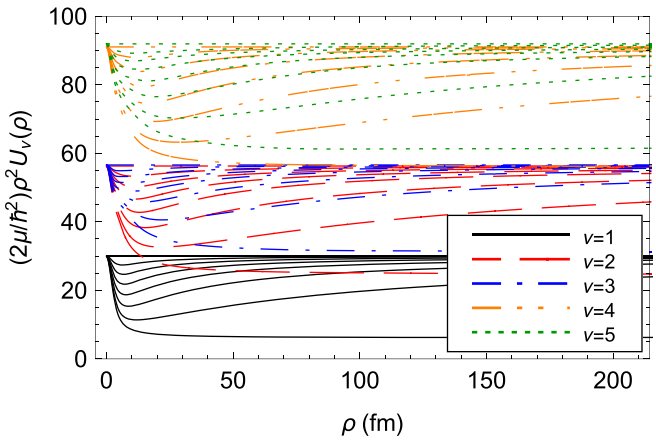

FIG. 10. The lowest five adiabatic potentials (ν=1–5) for the $4n$ system for the $J^\pi = 0^+$ symmetry with $L = 0$ using a single-Gaussian potential with $r_0 = 1.78$ fm. The strength V_0 is tuned to give different scattering lengths from 0 to infinity with no two-body bound state. Each set of potentials represent a different s-wave scattering length in this range.

converge to a different asymptotic coefficient of $1/\rho^2$ at unitarity ($a \to \infty$) than for finite or vanishing scattering length. This can be viewed as a generalized consequence of Efimov physics [24,35–37]. It is apparent from these figures that the lowest few potentials in each system asymptotically approach the corresponding noninteracting potentials as ρ^{-3}, where a is finite.

TABLE II. Long-range ($\rho \to \infty$) C_ν coefficients of the lowest few adiabatic potential for the $3n$ and $4n$ systems [see Eq. (10)]. Also provided is the effective angular momentum $l_{\text{eff,u}}$ at unitarity. Unitarity values from other references are presented as $l^{(\text{ref})}_{\text{eff,u}}$ for comparison. The error estimates in C_ν and $l_{\text{eff,u}}$ are obtained from fitting the potentials over different ranges in the hyperradius.

N	$(LS)J^\pi$	ν	l_{eff}	C_ν	$l_{\text{eff,u}}$	$l^{(\text{ref})}_{\text{eff,u}}$
3	$(1\frac{1}{2})\frac{3}{2}^-$	1	5/2	15.1(3)	1.275(5)	1.2727(1),[a] 1.2727[c]
		2	9/2	15.2(3)	3.861(5)	3.868,[b] 3.8582[c]
		3	13/2	77.7(3)	5.219(5)	5.229,[b] 5.2164[c]
		5	17/2	108(3)	7.555(5)	7.553[c]
4	$(00)0^+$	1	5	86.7(3)	2.017(5)	2.0091(4)[a]
		2	7	156(3)	4.455(5)	4.444(3)[d]
		3	7	61.1(3)	5.071(5)	5.029(3)[d]
		4	9	209(3)	6.974(5)	6.863(3)[d]
		5	9	87.8(3)	7.258(5)	7.121(3)[d]

[a]Values extracted from Table III of [54]. The ground-state energies of two-component Fermi gases at unitarity are extracted in the zero-range limit.

[b]Values extracted from Table I of [55]. Energies of a trapped two-component Fermi gas are computed using hyperspherical techniques and given for a Gaussian interaction with a range of 0.05 oscillator units.

[c]Value extracted from the transcendental equation represented by Eq. (7) in [56] for equal-mass fermions.

[d]Values extracted from Table II of [57]. Long-range coefficients extracted from hyperspherical potential curves for a four-fermion system using a Gaussian two-body interaction at unitarity.

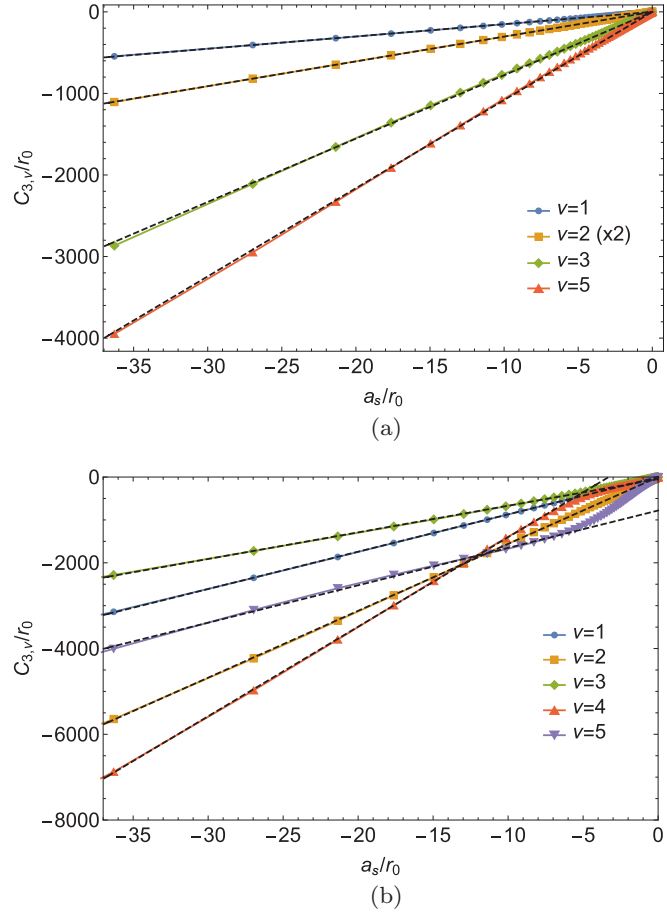

FIG. 11. The scattering length dependence of the three-body and four-body $C_{3,\nu}$ coefficients scaled by the range of the potential, r_0, for the lowest few potentials. In (a), the re-scaled $C_{3,\nu}$ coefficient is shown for the three-body case for the $(1\frac{1}{2})\frac{3}{2}^-$ symmetry. The circle, square, diamond, and triangle symbols represent the channels $\nu = 1$, 2, 3, and 5, respectively. The data for $\nu = 2$ are multiplied by a factor of 2, denoted by the label (×2), in order to differentiate between the data for $\nu = 1$ and $\nu = 2$. In (b), the re-scaled $C_{3,\nu}$ coefficient is shown for the four-body case for the $(00)0^+$ symmetry. The circle, square, diamond, upright triangle, and downward triangle symbols represent the channels $\nu = 1, 2, 3, 4$, and 5, respectively. The dashed lines are linear fits performed over the range $-36 < a_s/r_0 < -10$.

The scattering length dependence of $C_{3,\nu}$ is extracted from fitting the lowest adiabatic potentials to an inverse power-law expansion to $O(1/\rho^8)$ for each scattering length in the range $10 < \rho < 1500$ fm. The results of $C_{3,\nu}$ for the $3n$ and $4n$ systems are shown in Fig. 11. The figures show the scattering length dependence of $C_{3,\nu}$, rescaled by r_0, for the few lowest potentials using a single-Gaussian model for the two-body interactions with $r_0 = 1.78$ fm. There is clear evidence that the $C_{3,\nu}$ coefficient depends linearly on the s-wave scattering length for values of the rescaled s-wave scattering length $|a_s/r_0| > 10$, demonstrating universal physics at these scattering lengths. The rescaled s-wave scattering length for the nn

interaction is approximately, $|a_s/r_0| \approx 10.63$. The numerical values of $C_{3,\nu}$ are given in Table II. The deviations from the linear fits (near a_s/r_0 of -30) are due to errors in the extraction on the $C_{3,\nu}$ coefficient, which were estimated by performing the fits over varying ranges of $|a_s/r_0|$. As the scattering length increases, the ρ^{-3} behavior begins to dominate at larger and larger hyperradii, as seen in Figs. 9 and 10. In order to improve the accuracy of the value of $C_{3,\nu}$, the potentials would need to be computed out to larger values of ρ and better converged. Substituting the s-wave scattering length for the nn two-body interaction in the spin-singlet state ($a_s = -18.92$ fm for the AV8′ interaction) into the $C_{3,\nu}$ coefficients in Table II yields the expected long-range behavior for the lowest few adiabatic potentials that are relevant to understanding the low-energy behavior of the eigenphase shifts, discussed in Sec. VI.

VI. WIGNER-SMITH TIME DELAY

Starting from this understanding of the long-range behavior of the adiabatic potentials demonstrated in Sec. V, a full treatment of the energy-dependence scattering above the three-body and four-body continuum is now developed. To understand the 2016 experimental observation of a low-energy $4n$ signal by Kisamori *et al.*, a detailed analysis of the low-energy density of states is carried out. A simple way of quantifying the density of states is through a calculation of the Wigner-Smith time delay matrix, which for a single-channel calculation represents the amount of time incoming probability flux remains confined by the presence of a potential before escaping [58]. The Hermitian time delay matrix is defined in terms of the scattering matrix and its energy derivative as $Q(E) = i\hbar S dS^{\dagger}/dE$, which reduces to $Q(E) = 2\hbar d\delta(E)/dE$ for a single-channel calculation. It has been shown there is a direct relation between the total Wigner-Smith time delay and the density of states [59,60]. A peak in the time delay results from a rapid increase in the phase shift, usually over a small energy range. This occurs when the probability flux gets temporarily trapped for an extended period of time, interpreted usually as a resonance if there is an increase in phase of more than 2 radians.

In studying the elastic phase shift of the $3n$ and $4n$ systems, a comparison can be made between the phase shift with and without the inclusion of the second-derivative coupling term. Since the lowest adiabatic potential with the inclusion of the nonadiabatic diagonal second-derivative term provides a rigorous upper limit to the actual lowest potential, it would be intuitive to study how important this term is to the low-energy behavior. Also, a direct comparison will shed some light on the accuracy of treating the problem in the adiabatic approximation, without including any nonadiabatic couplings. This comparison for both $3n$ and $4n$ systems is shown in Fig. 12.

The single-channel elastic phase shift is shown for the $3n$ (lower curve) and $4n$ (upper curve) systems. These calculations were performed with and without the second derivative nonadiabatic coupling, being represented by the dashed and solid curves, respectively. There is surprising little change in the energy-dependence of the elastic phase shift in the energy range shown of $0 < E < 9$ MeV, with a noticeable difference starting around 2 MeV. There is a smooth rise in

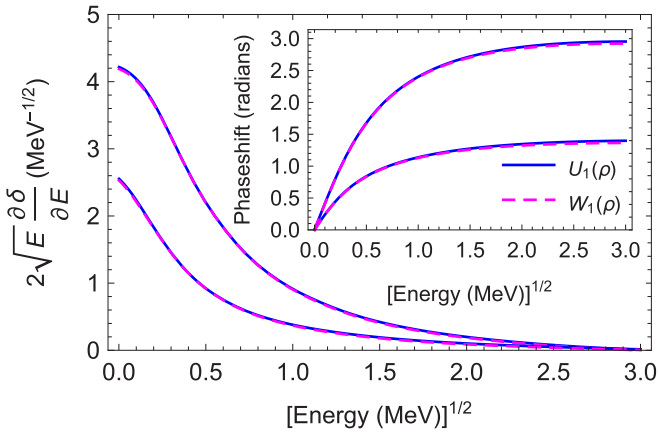

FIG. 12. The elastic phase shift (inset) and rescaled Wigner-Smith time delay in the lowest adiabatic potential for the $3n$ and $4n$ systems with and without the diagonal second-derivative coupling term, shown as dashed and solid lines, respectively. The upper curves are for the $4n$ system and the lower curves are for the $3n$ system.

the elastic phase shift for both the $3n$ and $4n$ systems with no peak in the energy derivative as one would expect for a true resonance. Instead, there is a low-energy enhancement of the density of states due to the divergent $1/\sqrt{E}$ behavior. The enhancement by $1/\sqrt{E}$ is a result of the long-range ρ^{-3} term in the potential. In accordance with the Wigner threshold law, the phase shift scales proportionally to the wave number k, leading to the enhancement in the energy derivative. In fact, it can be shown from the Born approximation that a potential of the form C/ρ^3 leads to a phase shift in the lth partial wave of $\delta_l(k) \approx -kC/[2l(l+1)]$.

From Fig. 12, there is little change in the energy behavior of the elastic phase shift and time delay for these few-neutron systems when excluding the nonadiabatic couplings, treating the problem in a purely adiabatic sense. In fact, only at large scattering energies ($E > 1.5$ MeV) is there any noticeable deviation in the energy dependence. The difference is due to the fact that the nonadiabatic second derivative couplings for

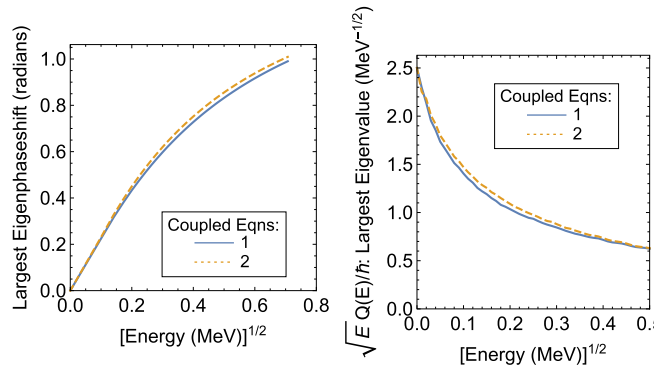

FIG. 13. The largest $3n$ eigenphase shift (left) and time delay (right) with the inclusion of 1 and 2 channels from a multichannel calculation to show the effects on the low-energy behavior from nonadiabatic coupling. These results use a single Gaussian model for the nn two-body interaction with the HH basis.

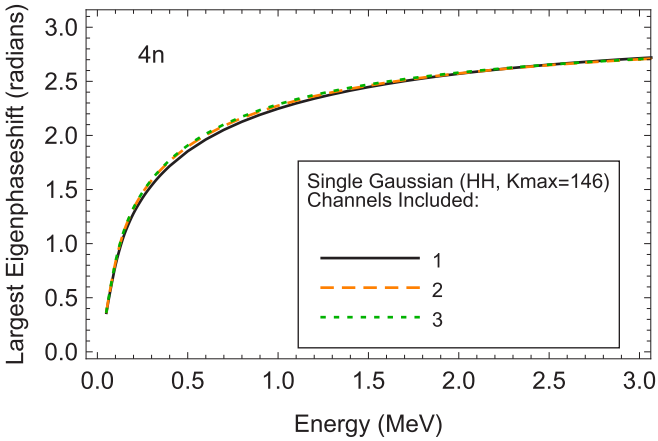

FIG. 14. The 4*n* phase shift in the lowest adiabatic potential with the inclusion of multiple channels an a multichannel calculation to show the effects on the low-energy behavior from channel coupling. These results use a single Gaussian model for the *nn* two-body interaction with the HH basis.

both systems are only appreciable at small ρ, corresponding to large energy, as seen in the previous section. A more thorough investigation into the affects of the nonadiabatic couplings is done by performing a multichannel calculation, including a few excited channels in solving Eq. (4) for scattering solutions.

Multichannel scattering calculations were performed for both neutron systems. Equation (4) was solved for the inclusion of a few coupled channels to compare the largest eigenphase shifts, which are shown in Figs. 13 and 14 for up to two and six channels for the 3*n* and 4*n* systems, respectively using the HH basis and a single Gaussian nuclear interaction. It is clear from these figures that the largest eigenphase shift shows little to no change in energy dependence at low-energies with increased number of included channels. The largest eigenphase shift using the AV8′ nuclear interaction and the CGHS basis is shown for up to 3 channels in Fig. 15. From these calculations with the realistic AV8′ interaction, the largest eigenphase shift does not change significantly at low energies with the inclusion of more channels. This negligible change is a result of the relatively weak and short-range behavior of the nonadiabatic coupling terms. From Sec. IV, it is shown the first-derivative couplings fall off as ρ^{-2} and second-derivative couplings fall off as ρ^{-4} at large hyperradii.

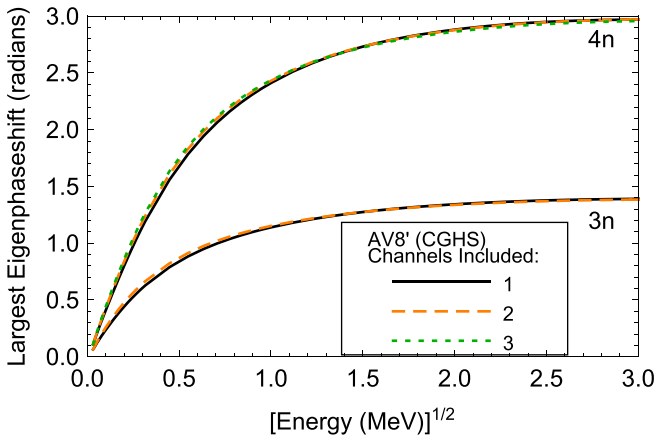

FIG. 15. Largest eigenphase shift for the 3*n* and 4*n* systems for the inclusion of up to three channels using the AV8′ interaction with the CGHS basis. The lowest curve is the single-channel results while the second lowest and highest curves are the resultant eigenphase shifts from a mutichannel calculation for two and three channels, respectively. The eigenphase shift is only slightly modified for energies less than 1 MeV, providing further support the adiabatic approximation is sufficient in describing the low-energy behavior.

VII. CONCLUSIONS

This article addresses a fundamental problem in few-body neutron interactions: whether a bound or resonant 4*n* state exists. The answer to this question is crucial for addressing the interpretation of a recent experiment by Kisamori *et al.* in 2016, which suggested evidence of a 4*n* resonance observed in the nuclear reaction $^4\mathrm{He} + {}^8\mathrm{He} \rightarrow 4n + {}^8\mathrm{Be}$ at an energy of 1.25 MeV above the four-neutron continuum [2]. This problem has been treated here using the adiabatic hyperspherical approach with realistic NN and 3N interactions with an emphasis on the AV8′ nuclear interaction with a CGHS basis and the AV18 interaction with a HH basis.

The 3*n* and 4*n* adiabatic hyperspherical potential curves were computed for the J^π states that provide the most attraction in each system, $\frac{3}{2}^-$ for the 3*n* system and 0^+ for the 4*n* system. A comparison was made between the adiabatic potentials computed in both basis sets, which show that the CGHS basis yields better converged potentials at large hyperradii. The lowest hyperspherical potential in each of these systems shows no qualitative feature that indicates the possible existence of a resonance. In fact, while these few neutron systems exhibit significant attraction, the potentials are still repulsive at all hyperradii due to strong Pauli repulsion.

The nonresonant behavior of these few neutron systems is further substantiated by a multichannel scattering treatment in the three-body and four-body continua with an analysis of the eigenphase shifts and Wigner-Smith time delay or density of states. It has been shown that the long-range behavior of the adiabatic potentials deviates from the noninteracting ρ^{-2} by an attractive ρ^{-3} behavior proportional to the *s*-wave scattering length. This attractive long-range term greatly influences the low-energy behavior of the eigenphase shifts, in turn leading to a $1/\sqrt{E}$ enhancement of dependence of the density of states at low energy. This enhancement of the density of states could suggest an explanation for the low-energy signature observed in the Kisamori *et al.* experiment in 2016 [2], despite the fact that there is no peak in the density of states and no rapid increase in the eigenphase shift of the type associated with a resonance. A multichannel treatment of few-neutron scattering was performed to include nonadiabatic coupling to excited states. This treatment showed little change in the energy-dependent phase shift in the energy region of interest, which demonstrates that these systems can be accurately treated in a nonadiabatic picture.

Universal physics has also been studied and shown to be relevant for understanding these few neutrons systems due to the large size of the s-wave scattering length relative to the range of the nn interaction. The fact that the adiabatic potentials computed using a simple Gaussian interaction agree accurately with those using the full AV8′ potential provides strong evidence that these systems exhibit universal physics. Furthermore, the $3n$ and $4n$ systems have also been treated with different realistic nucleon-nucleon interactions from chiral effective field theory using the HH basis. The potentials using these interaction models all show qualitative agreement in the region of hyperradii where the HH basis is well converged. The universal behavior in these systems has been elucidated by studying the scattering length dependence of the long-range behavior of the lowest few adiabatic potentials using a Gaussian two-body interaction. At large ratios of the s-wave scattering length to the range of the potential ($|a_s/r_0| \geqslant 10$), the long-range ρ^{-3} coefficient depends linearly on the scattering length, consistent with what is expected with a delta-function contact potential.

ACKNOWLEDGMENTS

Discussions with Emiko Hiyama and access to her unpublished Gaussian fitted AV8′ potential are much appreciated. The work done by M.D.H. and C.H.G. is supported in part by the U.S. National Science Foundation, Grant No. PHY-1912350, and in part by the Purdue Quantum Science and Engineering Institute.

[1] F. M. Marqués, M. Labiche, N. A. Orr, J. C. Angélique, L. Axelsson, B. Benoit, U. C. Bergmann, M. J. G. Borge, W. N. Catford, S. P. G. Chappell, N. M. Clarke, G. Costa, N. Curtis, A. D'Arrigo, E. de Góes Brennand, F. de Oliveira Santos, O. Dorvaux, G. Fazio, M. Freer, B. R. Fulton *et al.*, Detection of neutron clusters, Phys. Rev. C **65**, 044006 (2002).

[2] K. Kisamori, S. Shimoura, H. Miya, S. Michimasa, S. Ota, M. Assie, H. Baba, T. Baba, D. Beaumel, M. Dozono, T. Fujii, N. Fukuda, S. Go, F. Hammache, E. Ideguchi, N. Inabe, M. Itoh, D. Kameda, S. Kawase, T. Kawabata *et al.*, Candidate Resonant Tetraneutron State Populated by the ^{4}He(^{8}He,^{8}B) Reaction, Phys. Rev. Lett. **116**, 052501 (2016).

[3] N. K. Timofeyuk, Do multineutrons exist? J. Phys. G: Nucl. Part. Phys. **29**, L9 (2003).

[4] S. C. Pieper, Can Modern Nuclear Hamiltonians Tolerate a Bound Tetraneutron? Phys. Rev. Lett. **90**, 252501 (2003).

[5] C. A. Bertulani and V. Zelevinsky, Is the tetraneutron a bound dineutron–dineutron molecule? J. Phys. G: Nucl. Part. Phys. **29**, 2431 (2003).

[6] R. Lazauskas and J. Carbonell, Three-neutron resonance trajectories for realistic interaction models, Phys. Rev. C **71**, 044004 (2005).

[7] R. Lazauskas and J. Carbonell, Is a physically observable tetraneutron resonance compatible with realistic nuclear interactions? Phys. Rev. C **72**, 034003 (2005).

[8] A. M. Shirokov, G. Papadimitriou, A. I. Mazur, I. A. Mazur, R. Roth, and J. P. Vary, Prediction for a Four-Neutron Resonance, Phys. Rev. Lett. **117**, 182502 (2016).

[9] S. Gandolfi, H.-W. Hammer, P. Klos, J. E. Lynn, and A. Schwenk, Is a Trineutron Resonance Lower in Energy than a Tetraneutron Resonance? Phys. Rev. Lett. **118**, 232501 (2017).

[10] J. G. Li, N. Michel, B. S. Hu, W. Zuo, and F. R. Xu, Ab initio no-core Gamow shell-model calculations of multineutron systems, Phys. Rev. C **100**, 054313 (2019).

[11] E. Hiyama, R. Lazauskas, J. Carbonell, and M. Kamimura, Possibility of generating a 4-neutron resonance with a $t = 3/2$ isospin 3-neutron force, Phys. Rev. C **93**, 044004 (2016).

[12] K. Fossez, J. Rotureau, N. Michel, and M. Płoszajczak, Can Tetraneutron be a Narrow Resonance? Phys. Rev. Lett. **119**, 032501 (2017).

[13] A. Deltuva, Tetraneutron: Rigorous continuum calculation, Phys. Lett. B **782**, 238 (2018).

[14] A. Deltuva and R. Lazauskas, Tetraneutron resonance in the presence of a dineutron, Phys. Rev. C **100**, 044002 (2019).

[15] A. Deltuva and R. Lazauskas, Comment on "Is a Trineutron Resonance Lower in Energy than a Tetraneutron Resonance?" Phys. Rev. Lett. **123**, 069201 (2019).

[16] S. Gandolfi, H. W. Hammer, P. Klos, J. E. Lynn, and A. Schwenk, Reply to Comment on "Is a Trineutron Resonance Lower in Energy than a Tetraneutron Resonance?" Phys. Rev. Lett. **123**, 069202 (2019).

[17] E. Hiyama and M. Kamimura, Study of various few-body systems using Gaussian expansion method (GEM), Front. Phys. **13**, 132106 (2018).

[18] M. D. Higgins, C. H. Greene, A. Kievsky, and M. Viviani, Nonresonant Density of States Enhancement at Low Energies for Three or Four Neutrons, Phys. Rev. Lett. **125**, 052501 (2020).

[19] J. Botero and C. H. Greene, Resonant Photodetachment of the Positronium Negative Ion, Phys. Rev. Lett. **56**, 1366 (1986).

[20] C. D. Lin, Feshbach and Shape Resonances in the e-H $^1P^o$ System, Phys. Rev. Lett. **35**, 1150 (1975).

[21] K. Michishio, T. Kanai, S. Kuma, T. Azuma, K. Wada, I. Mochizuki, T. Hyodo, A. Yagishita, and Y. Nagashima, Observation of a shape resonance of the positronium negative ion, Nat. Commun. **7**, 11060 (2016).

[22] H. C. Bryant, B. D. Dieterle, J. Donahue, H. Sharifian, H. Tootoonchi, D. M. Wolfe, P. A. M. Gram, and M. A. Yates-Williams, Observation of Resonances near 11 eV in the Photodetachment Cross Section of the H^- Ion, Phys. Rev. Lett. **38**, 228 (1977).

[23] Y. Suzuki and K. Varga, *Stochastic Variational Approach to Quantum-Mechanical Few-Body Problems* (Springer, Heidelberg, 1988).

[24] S. T. Rittenhouse, J. von Stecher, J. P. D'Incao, N. P. Mehta, and C. H. Greene, The hyperspherical four-fermion problem, J. Phys. B: At., Mol. Opt. Phys. **44**, 172001 (2011).

[25] J. Mitroy, S. Bubin, W. Horiuchi, Y. Suzuki, L. Adamowicz, W. Cencek, K. Szalewicz, J. Komasa, D. Blume, and K. Varga, Theory and application of explicitly correlated gaussians, Rev. Mod. Phys. **85**, 693 (2013).

[26] K. Varga, Y. Suzuki, and J. Usukura, Global-vector representation of the angular motion of few-particle systems, Few-Body Syst. **24**, 81 (1998).

[27] K. M. Daily, R. E. Wooten, and C. H. Greene, Hyperspherical theory of the quantum Hall effect: The role of exceptional degeneracy, Phys. Rev. B **92**, 125427 (2015).
[28] J. Wang, Hyperspherical approach to quantal three-body theory, Ph.D. thesis, University of Colorado, Boulder, 2012 (unpublished).
[29] K. M. Daily, J. von Stecher, and C. H. Greene, Scattering properties of the $2e^-2e^+$ polyelectronic system, Phys. Rev. A **91**, 012512 (2015).
[30] K. M. Daily, Hyperspherical asymptotics of a system of four charged particles, Few-Body Syst. **56**, 809 (2015).
[31] J. Wang, J. P. D'Incao, Y. Wang, and C. H. Greene, Universal three-body recombination via resonant d-wave interactions, Phys. Rev. A **86**, 062511 (2012).
[32] R. B. Wiringa, V. G. J. Stoks, and R. Schiavilla, An Accurate nucleon-nucleon potential with charge independence breaking, Phys. Rev. C **51**, 38 (1995).
[33] M. Piarulli, L. Girlanda, R. Schiavilla, A. Kievsky, A. Lovato, L. E. Marcucci, S. C. Pieper, M. Viviani, and R. B. Wiringa, Local chiral potentials with Δ-intermediate states and the structure of light nuclei, Phys. Rev. C **94**, 054007 (2016).
[34] A. Baroni *et al.*, Local chiral interactions, the tritium Gamow-Teller matrix element, and the three-nucleon contact term, Phys. Rev. C **98**, 044003 (2018).
[35] J. P. D'Incao, Few-body physics in resonantly interacting ultracold quantum gases, J. Phys. B **51**, 043001 (2018).
[36] C. H. Greene, P. Giannakeas, and J. Pérez-Ríos, Universal few-body physics and cluster formation, Rev. Mod. Phys. **89**, 035006 (2017).
[37] P. Naidon and S. Endo, Efimov physics: A review, Rep. Prog. Phys. **80**, 056001 (2017).
[38] H. Suno and B. D. Esry, Adiabatic hyperspherical study of triatomic helium systems, Phys. Rev. A **78**, 062701 (2008).
[39] G. Hagen, P. Hagen, H.-W. Hammer, and L. Platter, Efimov Physics Around the Neutron-Rich ^{60}Ca Isotope, Phys. Rev. Lett. **111**, 132501 (2013).
[40] V. Efimov and E. G. Tkachenko, On the correlation between the triton binding energy and the neutron-deuteron doublet scattering length, Few-Body Syst. **4**, 71 (1988).
[41] A. Kievsky and M. Gattobigio, Efimov physics with $1/2$ spin-isospin fermions, Few-Body Syst. **57**, 217 (2016).
[42] M. Gattobigio, A. Kievsky, and M. Viviani, Embedding nuclear physics inside the unitary-limit window, Phys. Rev. C **100**, 034004 (2019).
[43] A. Kievsky, M. Viviani, M. Gattobigio, and L. Girlanda, Implications of Efimov physics for the description of three and four nucleons in chiral effective field theory, Phys. Rev. C **95**, 024001 (2017).
[44] A. Kievsky, M. Viviani, D. Logoteta, I. Bombaci, and L. Girlanda, Correlations Imposed by the Unitary Limit between Few-Nucleon Systems, Nuclear Matter, and Neutron Stars, Phys. Rev. Lett. **121**, 072701 (2018).
[45] C. A. Regal and D. S. Jin, Experimental realization of the BCS-BEC crossover with a Fermi gas of atoms, Adv. At. Mol. Opt. Phys. **54**, 1 (2007).
[46] J. von Stecher and C. H. Greene, Spectrum and Dynamics of the BCS-BEC Crossover from a Few-Body Perspective, Phys. Rev. Lett. **99**, 090402 (2007).
[47] B. S. Pudliner, V. R. Pandharipande, J. Carlson, S. C. Pieper, and R. B. Wiringa, Quantum Monte Carlo calculations of nuclei with $A < 7$, Phys. Rev. C **56**, 1720 (1997).
[48] S. C. Pieper, V. R. Pandharipande, R. B. Wiringa, and J. Carlson, Realistic models of pion-exchange three-nucleon interactions, Phys. Rev. C **64**, 014001 (2001).
[49] J. Carlson, V. Pandharipande, and R. Wiringa, Three-nucleon interaction in 3-, 4- and ∞-body systems, Nucl. Phys. A **401**, 59 (1983).
[50] S. C. Pieper, The Illinois extension to the Fujita-Miyazawa three-nucleon force, in *New Facet of Three Nucleon Force - 50 Years of Fujita Miyazawa Three Nucleon Force (FM50)*, Proceedings of the International Symposium on New Facet of Three Nucleon Force, 29–31 October 2007, edited by H. Sakai, K. Sekiguchi, and B. F. Gibson, AIP Conf. Proc. No. 1011 (AIP, New York, 2008), p. 143.
[51] M. Piarulli, A. Baroni, L. Girlanda, A. Kievsky, A. Lovato, E. Lusk, L. E. Marcucci, S. C. Pieper, R. Schiavilla, M. Viviani, and R. B. Wiringa, Light-Nuclei Spectra from Chiral Dynamics, Phys. Rev. Lett. **120**, 052503 (2018).
[52] Z. Zhen and J. Macek, Loosely bound states of three particles, Phys. Rev. A **38**, 1193 (1988).
[53] B. D. Esry and C. H. Greene, Validity of the shape-independent approximation for Bose-Einstein condensates, Phys. Rev. A **60**, 1451 (1999).
[54] X. Y. Yin and D. Blume, Trapped unitary two-component Fermi gases with up to ten particles, Phys. Rev. A **92**, 013608 (2015).
[55] D. Blume, J. von Stecher, and C. H. Greene, Universal Properties of a Trapped Two-Component Fermi Gas at Unitarity, Phys. Rev. Lett. **99**, 233201 (2007).
[56] F. Werner and Y. Castin, Unitary Quantum Three-Body Problem in a Harmonic Trap, Phys. Rev. Lett. **97**, 150401 (2006).
[57] J. von Stecher and C. H. Greene, Correlated Gaussian hyperspherical method for few-body systems, Phys. Rev. A **80**, 022504 (2009).
[58] F. T. Smith, Lifetime matrix in collision theory, Phys. Rev. **118**, 349 (1960).
[59] C. Texier, Wigner time delay and related concepts: Application to transport in coherent conductors, Physica E **82**, 16 (2016), special issue, Frontiers in quantum electronic transport – in memory of Markus Bttiker.
[60] M. Aymar, C. H. Greene, and E. Luc-Koenig, Multichannel Rydberg spectroscopy of complex atoms, Rev. Mod. Phys. **68**, 1015 (1996).